

# Suzaku-WAM soft gamma-ray all-sky monitor by the earth occultation technique

C.Kira<sup>1</sup>, Y.Fukazawa<sup>1</sup>, T.Asano<sup>1</sup>, T.Takahashi<sup>1</sup>, T.Uehara<sup>1</sup>, Y.Hanabata<sup>1</sup>, H.Takahashi<sup>1</sup>,  
K.Yamaoka<sup>2</sup>, M.Tashiro<sup>3</sup>, Y.Terada<sup>3</sup>, T.Tamagawa<sup>4</sup>, K.Makishima<sup>4,5</sup>,  
K.Nakazawa<sup>5</sup>, M.Ohno<sup>6</sup>, T.Takahashi<sup>6</sup>, M.Kokubun<sup>6</sup>, and HXD-WAM team

<sup>1</sup> Hiroshima Univ., <sup>2</sup>Aoyama Gakuin Univ., <sup>3</sup>Saitama Univ.

<sup>4</sup>RIKEN, <sup>5</sup>Univ. of Tokyo, <sup>6</sup>ISAS/JAXA

*E-mail(CK): kira@hep01.hepl.hiroshima-u.ac.jp*

## ABSTRACT

Suzaku-WAM has detected many gamma-ray bursts and solar flares. In addition, thanks to its large field of view, WAM is able to monitor the bright soft gamma-ray sources by the earth occultation technique, as CGRO-BATSE. We have constructed the analysis system of the WAM earth occultation, performed calibration by using spectra of the Crab nebula, and then found that the response uncertainty is around 10–20%. As a result, WAM is an important all-sky monitor in 50keV–1MeV band. This is unique against the RXTE/ASM (1–10keV) and Swift/BAT (10–100keV). Here, we introduce the analysis process, Crab calibration, and preliminary results on the Galactic black hole binaries and AGNs.

KEY WORDS: workshop: soft gamma-ray — black hole binary — Suzaku-WAM — earth occultation

## 1. Introduction

It is believed that most of black holes are accompanied by jets. So as to investigate the mechanism of jet emission, it is important to study non-thermal components of jet origin in soft gamma-ray region. However, still the soft gamma-ray emission from black holes is not well understood. In low/hard state, is there a non-thermal component or 511keV line associated with the jet emission beyond the normal thermal-Compton components? In high/soft state, where is a cut-off for the power-law component? How about very high state? In order to give an answer to these questions, it is essential to study spectral changes at the state transition. Hence, it is very important to monitor black holes continuously, especially in several 100 keV bands, and catch the state transition. Here we introduce the Suzaku-WAM soft gamma-ray all-sky monitor by the earth occultation technique, and show preliminary results on the black hole binaries and AGNs.

## 2. WAM ( Wide-band All-sky Monitor )

Suzaku-WAM (Wideband All-sky Monitor) is active shield of the HXD (Hard X-ray Detector) constructed from thick BGO scintillators and photomultipliers (Fig.1; Yamaoka et al. 2009, PASJ in press ). It surrounds four sides of HXD, and each side is called WAM0, WAM1, WAM2, and WAM3. WAM is also a detector with very large field of view ( $2\pi$  str), wide energy range (50–5000

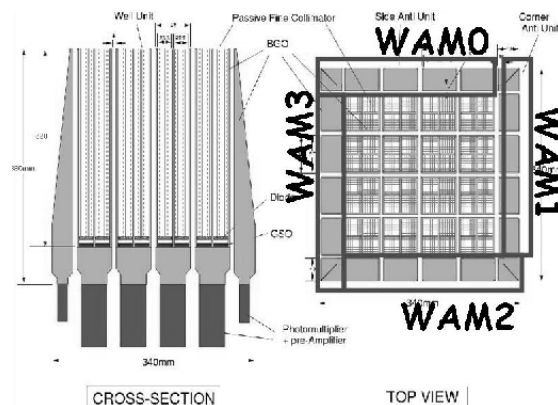


Fig. 1. Overview of Suzaku-WAM

keV), and large effective area ( $800 \text{ cm}^2$ ) to observe many gamma-ray bursts, soft gamma-ray repeaters, and solar flares. In addition, thanks to its large field of view, WAM can monitor bright soft gamma-ray sources of at least 50 mCrab with the earth occultation technique, as CGRO-BATSE (Ling et al. 2000, ApJS 127, 79). Current all-sky monitors are RXTE-ASM (1.5–12 keV) and Swift-BAT (15–150 keV). WAM is unique against such monitors for its high energy band, and enables us to monitor objects in wide energy band from 1keV to 600keV, by utilizing these three instruments. This is a great advantage to observe the hard tail of black hole binaries and search non-thermal components or 511keV line associated with

the jet ejection.

### 3. Analysis Procedure

#### 3.1. Calculate Occultation Time

At first, we selected the observations in which the incident angle of a target object to each WAM detector is smaller than 50 degrees, and calculate the time of occultation from target position and satellite orbit. There are about 15 occultations in one day, and each occultation is recognized by two steps of count rate at the begin and end of the occultation in the light curve. Fig.2 is an example of earth occultation of the Crab.

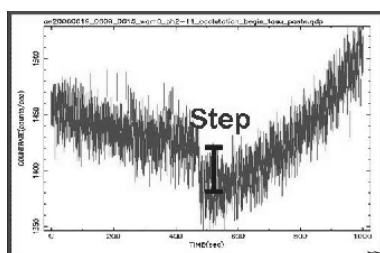


Fig. 2. Example of earth occultation step of the Crab

#### 3.2. Extract Occultation Light Curve

We analyzed Suzaku-WAM TRN-data. TRN-data are light curves of 55 energy channels with a time resolution of 1 sec. Here, we treated the light curves of 1–27 ch in 50–1000 keV, and extracted the light curve before/after 500 sec for each occultation in each energy channel.

#### 3.3. Sum over Light Curves

Since the earth occultation time calculated above is obtained without considering the atmospheric absorption, we must correct it before summing over the occultation light curves. The effect of atmosphere depends on the object track on the earth, seen from the satellite. Therefore, we obtained the relation between the real time of occultation and the duration of occultation. Using the obtained relation, we corrected the time from the duration of predicted occultation. We used only the data whose occultation duration time is longer than 1200 sec. We eliminated the occultation light curves containing SAA, background high-rate period, and calibration mode, and summing over the occultation light curves in one observation, one month, or three years for each energy channel to increase the statistics. WAM2 data are not in use because of its large calibration uncertainty

#### 3.4. Quantify Occultation Step Count Rate

We fitted an occultation light curve in each energy channel by an appropriate function to quantify the step count rate (Fig.3). Here, occultation light curves at the begin and end are simultaneously fitted with the same step

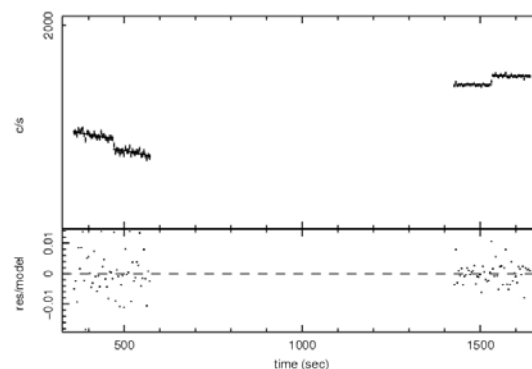


Fig. 3. Example of fitting earth occultation step of the Crab

count rate. We derived the spectrum of the object from the step count rates in each energy channel.

#### 3.5. Calculate the Response Function

We calculated the response functions from the incident direction of the object to the WAM. The response is created for one observation, during which incident direction is the same. In the case of the occultation light curves summing over one month or three years, we averaged the responses too, weighted by number of occultations in each observation.

### 4. Current detection uncertainty

Detection is almost limited by the photon statistics of background events. We analyzed the step count rate of 11 dark objects for WAM in the same method as above, and derived the systematic uncertainty of detection by estimating the variance of the obtained step count rates for these dark objects(Fig.4).

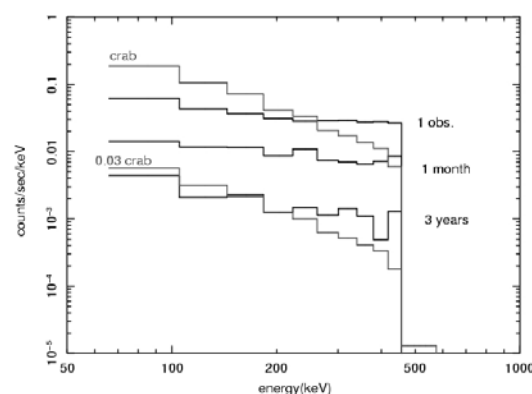


Fig. 4. Current detection uncertainty

Three-year integration gives systematic errors of 0.03 Crab at 100 keV. However, the analysis procedure is not yet polished well, and therefore the uncertainty is currently somewhat worse than the above.

## 5. Calibration by the Crab

The incident direction varies with the satellite attitude, and the WAM response function strongly depends on the incident direction due to the surrounding satellite body and other instruments. Therefore, we first calibrated the response function by the Crab for various incident directions. As shown in Fig.4, in three-year integration, Crab can be detected up to 300 keV in one observation integration, during which the satellite attitude is the same.

We fitted the spectrum of each observation by power-law model with a photon index fixed to 2.1, and obtained the flux in 100-800keV. We confirmed that the flux does not depend on the elapsed time from launch. On the other hand, it is significant that the flux depends on the incident angle to each WAM detector above 60 degrees. The flux obtained by WAM1 add WAM3 is found to be systematically different from that of WAM0 by several tens %, and thus we corrected the difference.

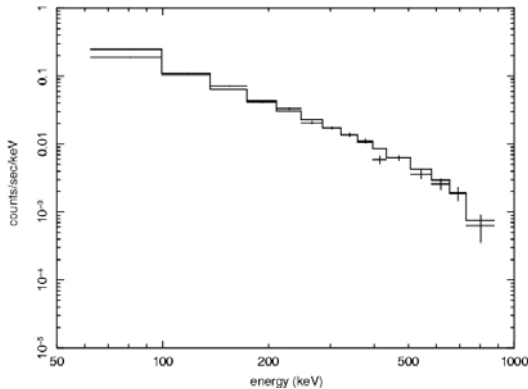


Fig. 5. Averaged spectrum of the Crab in three-year integration

In three-year integration, it can be detected up to 800 keV (Fig.5). The spectrum is well fitted by power-law model with a photon index of 2.1 and flux of  $1.1 \times 10^{-8}$  erg/sec/cm<sup>2</sup> (100–500 keV) with a 30% uncertainty. These are consistent with the INTEGRAL results (Sizun et al. 2004, astro-ph/0406052, Proc. of the 5th INTEGRAL Workshop).

## 6. Preliminary Results

### 6.1. Long-term Light Curve of Cyg X-1

The long-term light curve in one observation integration of Cyg X-1 is successfully obtained in 100–600 keV with WAM as shown in Fig.6. Together with light curves of RXTE-ASM and Swift-BAT, we can clearly see the different behavior between them. Noticeably, the bright phase in 2006 September (MJD $\approx$ 53400) is coincident with a high energy gamma-ray detection at 0.1–1 TeV energies by MAGIC telescope (Albert et al. 2007, ApJ, 665, L51). This event was also reported by RXTE-ASM, Swift-BAT and INTEGRAL-IBIS and SPI (Malzac et al.

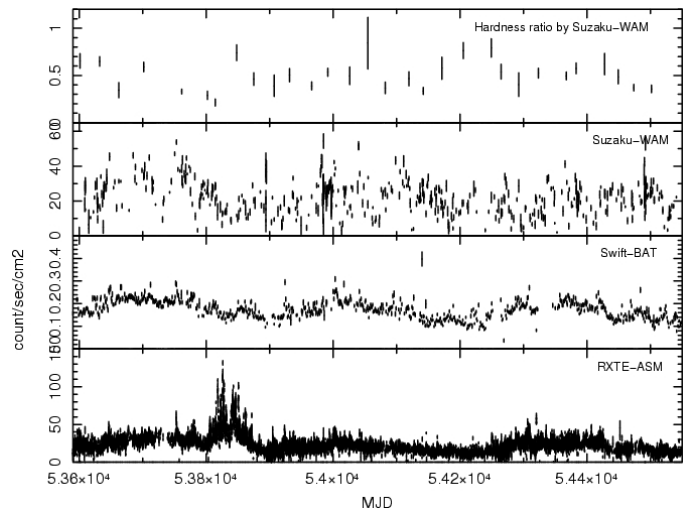


Fig. 6. Long-term light curve of Cyg X-1

2008, astro-ph/0805.4391v1). The next noticeable is a dark phase above 10 keV against a bright flare in 2006 April–May (MJD $\approx$ 53830). Although there is no report that Cyg X-1 became high state in this period, it shows a typical high state feature.

### 6.2. Spectra of Cyg X-1 at Various Epochs

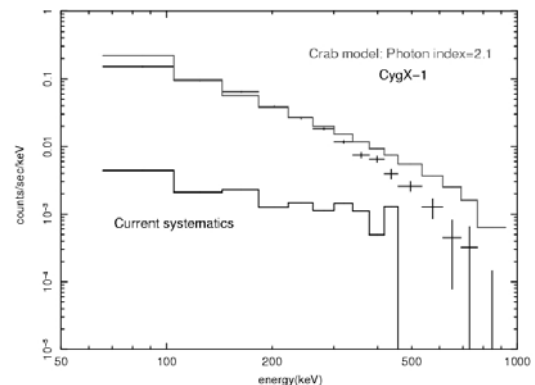


Fig. 7. Averaged spectrum of Cyg X-1 in three-year integration

Fig.7 shows the average spectrum in three-year integration of Cyg X-1, compared with the spectrum of the Crab with a photon index of 2.1. High energy cut-off is clearly seen. It is well fitted by cut-off power-law model with a photon index of 1.5 and a cut-off at 200 keV.

Time resolved spectra can be obtained up to 400–500 keV in each month as shown in Fig.8–11. Thus we can trace a spectral change of Cyg X-1. Fig.8 is a period during which Cyg X-1 seems like a high state in 2006 April (MJD $\approx$ 53830), Fig.9 is a period of TeV gamma-ray flare in 2006 September (MJD $\approx$ 53400), Fig.10 is a period of soft gamma-ray flare in 2007 August (MJD $\approx$ 54300; Golenetskii et al. 2007, GCN CIRCULAR 6745), and

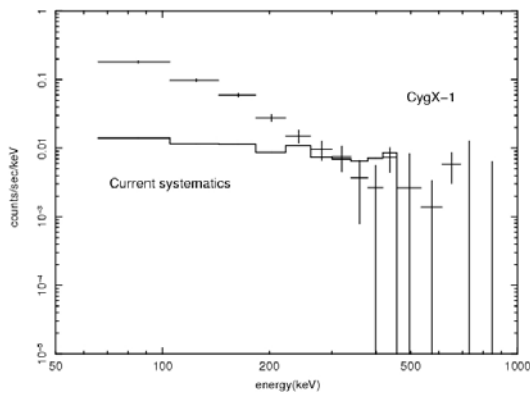


Fig. 8. Spectrum of Cyg X-1 (20060319–20060407)

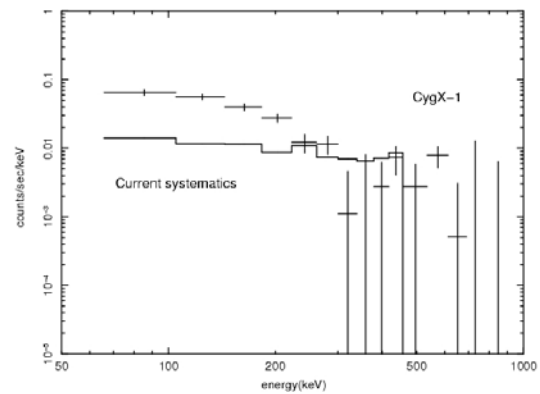


Fig. 10. Spectrum of Cyg X-1 (20070711–20070808)

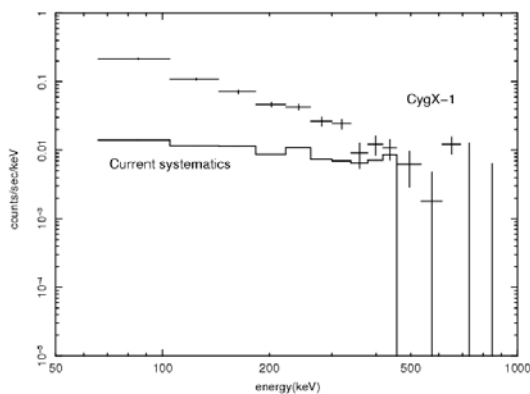


Fig. 9. Spectrum of Cyg X-1 (20060913–20061010)

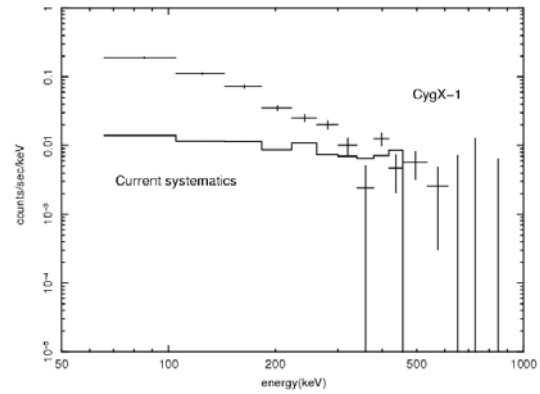


Fig. 11. Spectrum of Cyg X-1 (20080108–20080203)

Fig.11 is a period during which the flux is at the average level in 2008 January (MJD $\simeq$ 54480). Compared with Fig.11 or averaged spectrum (Fig.7), the spectrum in high-state-like period seems softer and that in the TeV flare period is harder.

### 6.3. Other Sources

We obtained a monthly light curve and spectrum of GRS 1915+105 as shown in Fig.12. While the count rate of Swift is almost the half of Cyg X-1, the flux above 100 keV is much smaller for GRS 1915+105, although the detection is significant. During the normal hard state before MJD $\simeq$ 54250, GRS 1915+105 was continuously detected. After entering the soft state, the detection becomes difficult. During the soft state, several outbursts occurred, and WAM detected one of them at 0.5 Crab level around MJD $\simeq$ 54380.

Fig.13 shows the average spectrum of GRS 1915+105 in three-year integration. It is detected up to 300 keV, and the photon index is around 2. Fig.14 shows the spectrum at the outburst at MJD $\simeq$ 54380. Even in only one-month integration, it is detected up to 300 keV. The spectral shape is not so different from the average. Other black hole binaries are also detected, such as GX 339-4,

together with AGNs such as Cen A and NGC 4151.

### References

- Albert et al. 2007, ApJ, 665, L51
- Golenetskii et al. 2007, GCN CIRCULAR 6745
- Ling et al. 2000, ApJS 127, 79
- Malzac et al. 2008, astro-ph/0805.4391v1
- Sizun et al. 2004, astro-ph/0406052, Proc. of the 5th INTEGRAL Workshop
- Yamaoka et al. 2009, PASJ in press

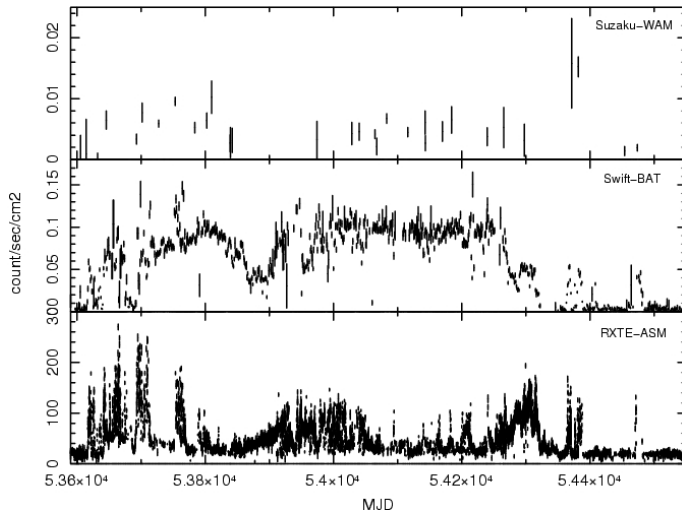


Fig. 12. Monthly light curve of GRS 1915+105

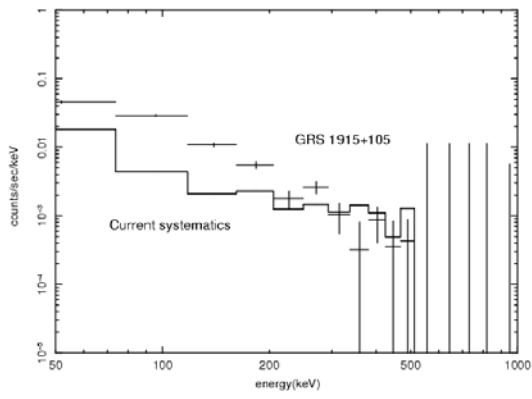


Fig. 13. Averaged spectrum of GRS 1915+105 in three-year integration

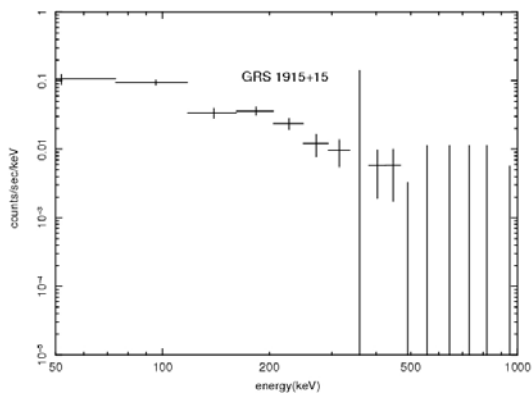


Fig. 14. Spectrum of GRS 1915+105 at flare period on MJD 54380